J Porous Mater (2015) 22:1407–1416
DOI 10.1007/s10934-015-0020-z

Facile one-step synthesis of micro/mesoporous material with ordered bimodal mesopores templated by protic ionic liquid as a heterogeneous catalyst support for alkylation

Shuo Zhao[1] · Xiaoli Sheng[1] · Yuming Zhou[1] · Man He[1] · Xiaoqin Fu[1] · Yiwei Zhang[1]

Published online: 16 July 2015

Abstract Nanosized hierarchical micro/mesoporous composites were successfully fabricated using non-ionic block copolymer Pluronic P123 and protic ionic liquid (butylamine acetate) as the co-templates. The obtained samples were characterized by several techniques, including small angle X-ray scattering, N_2 gas sorption, scanning electron microscope and transmission electron microscopy. The result established that the final silica materials possessed a disordered population of micropores coexisting with two different mesoporous channels of 4.0 and 7.3 nm. The formation mechanism of the micro/mesoporous silica which is based on the interaction between PIL and P123 is tentatively elucidated. 12-Tungstophosphoric acid catalysts incorporated into these micro/mesoporous materials were prepared by impregnation, and their catalytic performances were investigated in the alkylation of *o*-xylene with styrene. Alkylation results exhibited that all the catalysts showed the high catalytic performance in terms of propane conversion and selectivity to propene.

Keywords Micro/mesoporous material · Protic ionic liquid · P123 · Alkylation · Catalysis stability

✉ Yuming Zhou
ymzhou@seu.edu.cn

[1] Jiangsu Optoelectronic Functional Materials and Engineering Laboratory, School of Chemistry and Chemical Engineering, Southeast University, Nanjing 211189, People's Republic China

1 Introduction

Hierarchical porous silica materials have received significant attentions owing to their unique structure since the discovery of M41S by researchers from Mobil Oil in 1992 [1]. Hierarchical porous silica materials, combing the advantages of mesoporous materials with microporous materials, possess many excellent properties, such as high surface area, large pore volumes, high thermal, hydrothermal and mechanical stability [2, 3]. And these materials are widely studied as catalysts [4], adsorbents [5] and drug delivery carriers [6] so on. During the past decades, various methods have been put forward to obtain micro/mesoporous materials [7, 8]. And each of these methods allows that the other parameters can be altered and controlled. Thus, it is very important to choose an appropriate synthesis method to obtain the micro/mesoporous material. Among them, the approach using templates has been regarded as one of the most promising ways to obtain these hierarchical porous silica materials [9]. These templates include surfactants, emulsions, and colloids and so on [7, 8]. The appropriate templates are crucial due to the importance of the interaction between templates and siliceous precursors.

Ionic liquids (ILs) are molten salts at room temperature, in which ions are present. Recently, ILs attract an increasing interest in all kinds of fields because of their unique properties such as low vapor pressure, mild reaction condition, solvating ability, easy recycle ability and so on [3, 10–12]. Therefore, ILs can play roles in chemistry, organometallic, biocatalyzed reactions or other fields [13, 14]. It is said that ILs can act as multiple roles of cosolvent, cosurfactant as well as salt in the system [15]. And ILs can self-assemble into ordered structures like surfactants [16] in an aqueous solution because ILs comprise both a hydrophilic ionic head group and a hydrophobic organic

chain. On one hand, ILs may greatly affect the aggregation behavior of aqueous surfactant solution; on the other hand, ILs can act as the template to induce micro or mesoporous materials [17, 18].

In the previous work, micro/mesoporous materials have been synthesized by imidazolium based ILs. Hu et al. [19]. synthesized a high-quality cubic gyroid mesoporous silica (MCM-41) with the ionic liquid 1-hexadecyl-3-methylimidazolium bromide as the template under basic condition. Monolithic mesoporous silica with worm-like mesopore systems has been synthesized by Zhou et al. [18]. using $[C_4mim]^+BF_4^-$ as the template. Gao et al. [20]. successfully synthesized the micro/mesoporous silicate materials using P123 and imidazolium ILs ($[C_nmim]X$). They investigated the influence of the alkyl chain length, the different types of anions, and the hydrophobicity of $[C_n mim]X$ to the structure of final materials. And all the samples obtained had one kind of ordered mesoporous channels with a number of disordered micropores. Hence, it is generally possible to use ILs as template during the synthesis of micro/mesoporous silica materials.

Protic ionic liquids (PIL) are formed via the proton transfer from a Bronsted acid to a Bronsted base. In addition, many PILs are miscible with water to form mixtures at any composition, and these ions favorably form hydrogen bonds with water [21–23]. Whereas, the synthesis of micro/mesoporous silicate materials by a hydrothermal method has rarely been reported using PILs, and these materials just possess one kind of ordered mesopore channels. Chen et al. [24]. reported that the hierarchically nanostructured silica materials were synthesized by using protic ionic liquid (ethylammonium nitrate) and non-ionic block copolymer Pluronic P123 as templates. These materials had a disordered population of micropores and an ordered population of mesopores with one kind of pore range. Moreover, the micropores were caused by ethylammonium nitrate. The micro/mesoporous materials, combining the advantages of mesoporous materials and microporous materials, are expected to be more suitable for catalytic reactions as catalysts support material. 1-phenyl-1-xylyl ethane (PXE), which is the product of Friedel–Crafts alkylation of *o*-xylene and styrene, is a colorless synthetic liquid with many excellent properties suitable for various applications. 12-Tungstophosphoric acid (HPW) and ordered mesoporous SBA-15 are usually used as acid catalysts and support, respectively to obtain PXE [25–27]. Sheng et al. [28] successfully loaded HPW onto sulfonate-functionalized ionic liquid-modified mesoporous silica SBA-15 by total anion-exchange. And the final catalyst showed a high efficiency in alkylation. Thus, the traditional supports can be replaced by the micro/mesoporous materials to synthesize PXE to investigate if micro/mesoporous materials have an advantage for this reaction.

In this work, a new approach to prepare miro/mesoporous silica materials possessing both disordered micropores and two different kinds of mesoporous channels has been suggested. The porous silica materials were synthesized with P123 and PIL (butylamine acetate) as the co-templates by the hydrothermal method. A series of samples were synthesized by changing the PIL to P123 weight ratio and temperature during synthesis. Moreover, HPW supported on micro/mesoporous materials were prepared by impregnation method. The catalytic properties of the catalysts were assessed in the alkylation of *o*-xylene with styrene.

2 Experimental section

2.1 Chemicals

P123 ($PEO_{20}PPO_{70}PEO_{20}$) was purchased from Sigma-Aldrich, The inorganic silica precursor was silicon (IV) tetraacetate (TEOS 97 %, Fluka) and HCl (37 % in water, Aldrich) was used as reaction catalyst, butylamine (Merck) and acetic acid (Merck) were used to synthesise PIL.

2.2 Preparation of PIL

Butylamine acetate was obtained according to the literature [29]. A typical polymerization procedure is described as follows. Acetic acid (30.025 g) was added dropwise into butylamine (36.57 g) at 353 K. After stirring for 5 h, PIL which was colorless and viscous liquid was obtained. PIL was characterized by ^{1}H NMR. ^{1}H-NMR ($CDCl_3$) δ: 9.916 (s, 1H, $–NH_3^+$), 2.58 (s, 3H, $CH_3COO–$), 1.4 (s, 2H, $–CH_2^-$), 0.7 (s, 3H, $–CH_3$), which is consistent with literature reports.

2.3 Synthesis of micro/mesoporous materials

In a typical synthesis, 4 g P123 and an appropriate amount of PIL were completely dissolved in water; its pH was controlled by HCl (2 M). 9 g tetraethyl orthosilicate (TEOS) was then dripped slowly with stirring. After stirring at 313 K for 24 h, the whole solution was transferred into an autoclave for aging at an appropriate temperature for 48 h. The white as-synthesized solid powders were then calcined at 823 K for 6 h in ambient air, with a heating rate of 3 K min^{-1}.

Similarly, a series of micro/mesoporous materials were synthesized by changing the ratio of PILs and temperature during synthesis. The final products were denoted as PIL-X–Y, in which X represents the mass ratio of PIL to (P123 + PIL); Y represents the aging temperature, respectively. As a comparison, samples either without P123

(denoted as PIL) or using water to replace PIL (denoted as P123) were also prepared.

2.4 Catalysts preparation

1 g of micro/mesoporous materials were added into the mixture of 20 mL ethyl alcohol and 0.4 g of 12-Tungstophosphoric acid at 333 K. The mixture continuously stirred until ethyl alcohol steamed. The obtained white solid was dried at 393 K overnight and calcined in air at 573 K for 4 h.

2.5 Catalytic tests

The alkylation reactions were carried out in a continuously stirred oil batch reactor under 393 K. Styrene (6 g), *o*-xylene (45 g) (quality ratio of *o*-xylene to styrene, 7.5:1) and 1.02 g of catalyst were introduced in a three-neck 100 mL round-bottom flask equipped with a condenser for 3 h. The mixture of the small amount of *o*-xylene was initially added to the round-bottom flask at 393 K, followed by the desired amount of catalyst, the mixture of a certain amount of styrene and the remaining *o*-xylene then dropwise into the flask for 2 h. The final reaction mixture remained for another 1 h. After the reaction, unreacted *o*-xylene was distilled out under atmospheric pressure, and then the obtained liquid was denoted by crude product which was analyzed with GC-9890A gas chromatograph equipped with OV-1 capillary column and a flame ionization detector (FID). The yield of PXE was defined as follows:

$$\text{Yield of PXE } (\%) = \frac{\text{actual product weight}}{\text{theoretical product weight}} \times 100\%$$

$$\text{Actual product weight} = \text{crude product weight} \times \text{PXE (chromatography)}\ \%$$

2.6 Characterization

The structure of the calcined samples was characterized by an X-ray powder diffractometor (Rigaku, RINT-Ultima III) using Cu Kα radiation with 40 kV and 200 mA. All scans were continuous and run between 2θ values of 0–5°. The N_2 physical adsorption and desorption isotherms were adopted at 77 K to obtain surface areas with ASAP 2020 apparatus (Micromertics USA) by means of the Brunauer-Emmett-Teller (BET) method. The pore size distribution in mesopore range was analyzed by the BJH (Barrett-Joyner-Halenda) method using the Halsey equation for multilayer thickness. Micropore volume was calculated by the t-plot method. Transmission Electron Microscopy (TEM) was performed on FEI Tecnai G20 instrument. Infrared spectra were recorded on a Bruker Tensor 27 (German) using DRIFT techniques, scanned from 4000 to 400 cm^{-1}. The sample was ground with KBr and pressed into a thin wafer. The samples were evacuated at 573 K for 4 h before the measurement. Scanning electron microscopy (SEM) images were recorded on a JEOL JSM-5600L SEM Instrument with a working distance of 3–4 mm and an electron voltage of 3.0 kV.

3 Results and discussion

3.1 Effect of the PIL content

Figure 1 shows the XRD patterns of the samples induced by PIL/P123 co-templates at the aging temperature of 393 K. Three well-resolved diffraction peaks which include a strong reflection at $2\theta = 0.86°$ for d_{100} and two other weaker reflections at $2\theta = 1.55°$ and $2\theta = 1.71°$ respectively for d_{110} and d_{200} are clearly observed in the curves of P123, PIL-30, PIL-40, PIL-50, which are the characteristic peaks of hexagonal arrangement of SBA-15. Only one broad diffraction peak (100) with a much lower intensity is preserved for PIL-60, indicating its structure lack orderliness. No other obvious diffraction peak is observed with increasing PIL concentration, stating a poor order degree for PIL-70. The results show that the samples induced by P123/PIL co-templates can keep the ordered structure under the low PIL content. With the increase of PIL content, the characteristic peaks of hexagonal arrangement of SBA-15 gradually disappear and the structure of the final materials becomes disordered. This phenomenon makes known that an appropriate PIL content is good for the order degree of the final structure.

Figure 2a shows the N_2 adsorption–desorption isothermals of calcined materials at 393 K. Obviously, all the

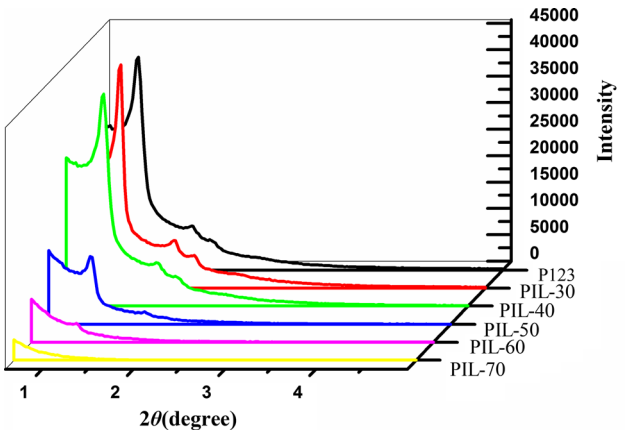

Fig. 1 XRD patterns of the samples induced by PIL/P123 co-templates at 393 K

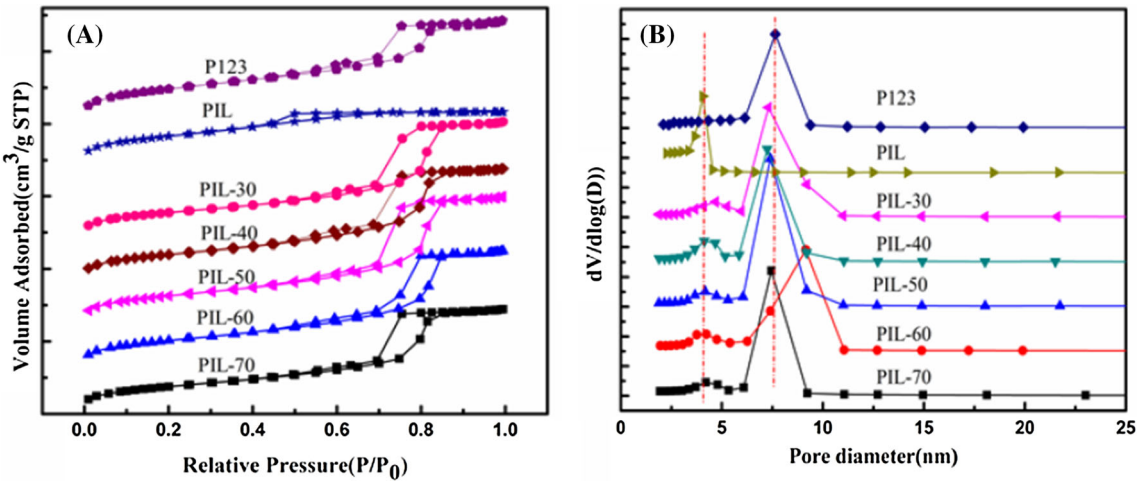

Fig. 2 **a** N_2 adsorption–desorption isotherms, **b** pore size distributions calculated by BJH model based on desorption curves of the calcined samples induced by P123/PIL co-templates at 393 K

Table 1 Physicochemical properties of the calcined samples induced by P123/PIL co-templates at 393 K

Sample name	BET surface area (m^2/g)	Pore volume of smaller mesopores (cm^3/g)	Pore volume of larger mesopores (cm^3/g)	Average pore size (nm)
PIL-30	684	0.25	1.01	7.36
PIL-40	730	0.28	0.94	6.71
PIL-50	781	0.24	1.15	7.10
PIL-60	754	0.30	0.97	6.76
PIL-70	686	0.23	0.89	6.52
PIL	781	–	–	3.03
P123	881	–	–	5.01

adsorption isotherms exhibit the typical IV adsorption with a pronounced hysteresis loop which indicates the intersection network of mesoporous structures. At very low relative pressure p/p_0, an increase at the adsorption isothermal of all materials proves the presence of micropores. The pressure onset of the hysteresis keep at about 0.5, which illustrates pore size is barely influenced by the increase of PIL content. Meanwhile, it is worth noting that there is a clear hysteresis loop in the isothermals of PIL, indicating protic ionic liquid can self-assemble to micelles which act as the mesoporous templates at higher PIL concentration.

Figure 2b shows the pore size distribution calculated by BJH model based on desorption curves. Two peaks are clearly seen from the pore size distributions of all the samples, indicating materials have two different mesopore ranges of pores of 4.0 and 7.3 nm, which induced by PIL micelles and P123 micelles, respectively. From the data above, it is evidently found that pore size of PIL-60 shifts to 9.1 nm, which may be due to the existence of the mixed micelles of PIL and P123. From the date above, it can be found that PIL and P123 are miscible in the aqueous solution and can form mixed micelles at lower PIL concentration, moreover, PIL micelles can separated from the mixed micelles with the increase of PIL concentration. Thus, two different scale micelles which induce the micro/mesoporous material with two kinds of mesopores are formed. That certifies the function of ionic liquid for the material structure. Including, the ionic liquids which enter into the P123 micelles and self-assembly form the micelles play a role of mesoporous template, the other dissociative molecules may act as the microporous template.

The characteristic data on the samples are summarized in Table 1. From Table 1, It is shown that the total surface area of the sample PIL-50 is very large, as high as 781 $cm^3\ g^{-1}$. And the average pore size of each sample is larger than the sample P123, which gives more evidence that PIL and P123 can form the mixed micelles due to the hydrogen bond. Among them, PIL-50 possesses extremely large pore volume, which are larger than that of the others.

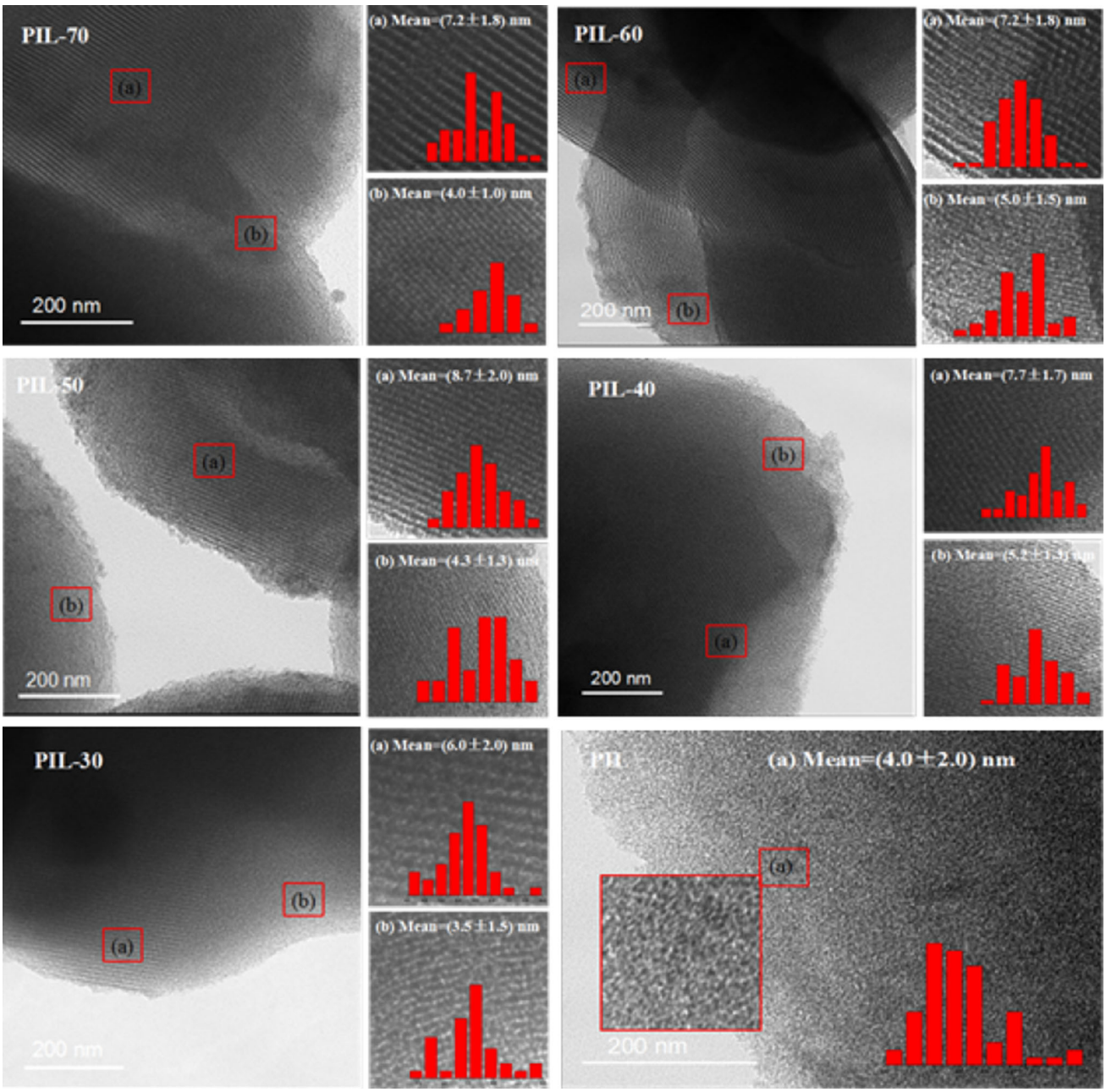

Fig. 3 The TEM images of the calcined samples induced by P123/PIL at 393 K. The pictures on the right of each image are the local enlargements with the same enlargement scale. *Insets* in each picture were the size distribution histograms

This phenomenon gives intuitive evidence that the positive contributions of PIL to the volume (Fig. 3).

The TEM images of the calcined samples prepared at 393 K show the structure of the samples obtained with different PIL content, meaning P123/PIL templates can induce micro/mesoporous composites with two kinds of mesoporous channels. All the images show very ordered mesoporous structure, these mesopores have two different pore size, including the large pore diameter at about 7.3 nm induced by the mixed micelles of PIL and P123 and the small pore diameter at about 4.0 nm induced by PIL micelles. The last image of PIL shows that there are numbers of disordered mesopores whose pore diameter is about 4.0 nm, which is consistent with the N_2 gas sorption result. Moreover, it gives evidence that the ordered mesoporous channels whose pore size is about 4.0 nm are induced by PIL micelles. It is worth noting that the sample PIL shows a disordered structure, while other samples using P123 exhibit the ordered mesoporous channels. This phenomenon may be explained by the fact that there is a

synergistic effect between P123 and PIL. PIL micelles can be arranged in order with the presence of P123 micelles. Namely, PIL can induce the ordered channels under the help of P123. And the micro/mesoporous materials with ordered bimodal mesopores are obtained due to the existence of P123 micelles and PIL micelles.

3.2 Effect of the hydrothermal temperature

The low-angle XRD patterns of the samples induced by PIL/P123 co-templates at different temperature are shown in Fig. 4. When the temperature is 393 and 373 K, three well-resolved diffraction peaks are observed in the curve, which corresponding to the (100), (110) and (200) reflections. Especially, the intensity of PIL-40-373 is much lower than PIL-40-393. When the temperature decreases to 353 K, three peaks are disappeared, indicating the sample's structure is disordered because of the low temperature. In summary, the temperature plays an important role on the final mesoporous structure, and too low temperature has a bad influence to the synthesis of ordered structure. Thus, an appropriate temperature is a significant requirement to obtain the desired material.

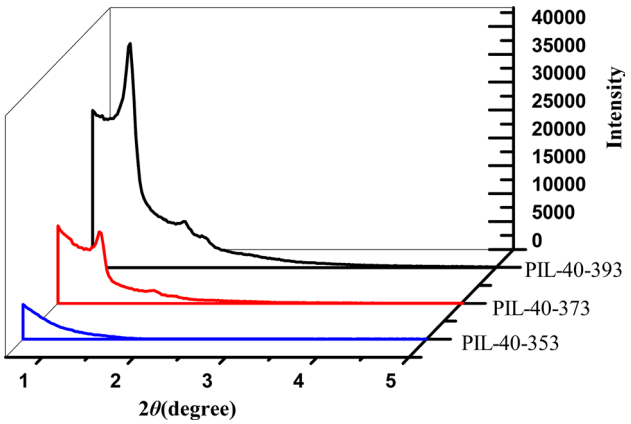

Fig. 4 XRD patterns of the PIL-40 at different temperature

Figure 5a shows the N_2 adsorption isotherms of the calcined samples at different hydrothermal temperature. Pronounced hysteresis loop characterizing the cylindrical mesopores can be observed at 393 or 373 K, representing that the samples have an ordered porous structure. However, in a sharp contrast, the adsorption of PIL-40-393 is higher than that of PIL-40-373, indicating the order degree of PIL-40-393 is better than PIL-40-373. At very low relative pressure p/p_0, an increase at the adsorption isothermal of samples proves the presence of micropores. The distortion of hysteresis loop indicates the loss of the ordered pore structure at 353 K, which is in agreement with the XRD results. Figure 5b shows the pore size distribution calculated by BJH model based on desorption curves. The average diameter of the mesopore is in a range of 6.5–7.2 nm. Furthermore, the diameter of the pore increases with the increase of reaction temperature. From the Table 2, it is can be seen that PIL-40-353 has a t-plot micropore area of 246 $m^2\ g^{-1}$, which is larger than other samples. When the temperature increases to 393 K, there is still a t-plot micropore area of 38 $m^2\ g^{-1}$, certifying the effect of PIL microporous template. On the basis of the above experimental results and the theory analysis, it is concluded that PIL-40-373 which not only possesses numbers of micropores but also remains the hexagonally ordered array structure are induced at a low temperature of 373 K, which demonstrates that the hydrothermal temperature is a significant factor to obtain the micro/mesoporous material.

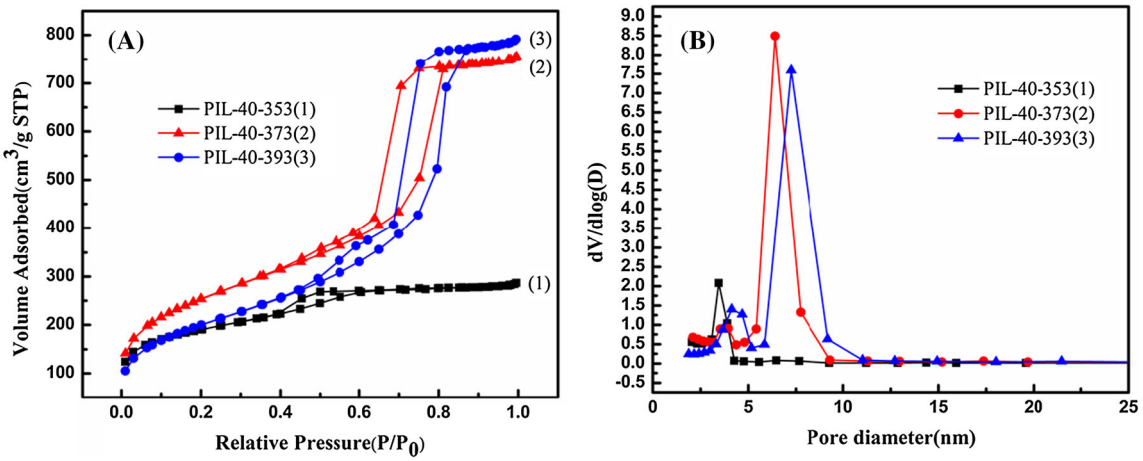

Fig. 5 **a** N_2 adsorption–desorption isotherms, **b** pore size distributions calculated by BJH model based on desorption curves of the calcined samples induced by PIL-40 co-templates at different temperature

Table 2 Physicochemical properties of the calcined samples induced by PIL-40 co-templates at different temperature

Sample name	BET surface area (m^2/g)	Micropore surface area (m^2/g)	Pore volume of smaller mesopores (cm^3/g)	Pore volume of larger mesopores (cm^3/g)	Average pore size (nm)
PIL-40-353	668	246	0.11	0.33	2.65
PIL-40-373	916	102	0.23	0.94	5.10
PIL-40-393	730	38	0.28	0.94	6.71

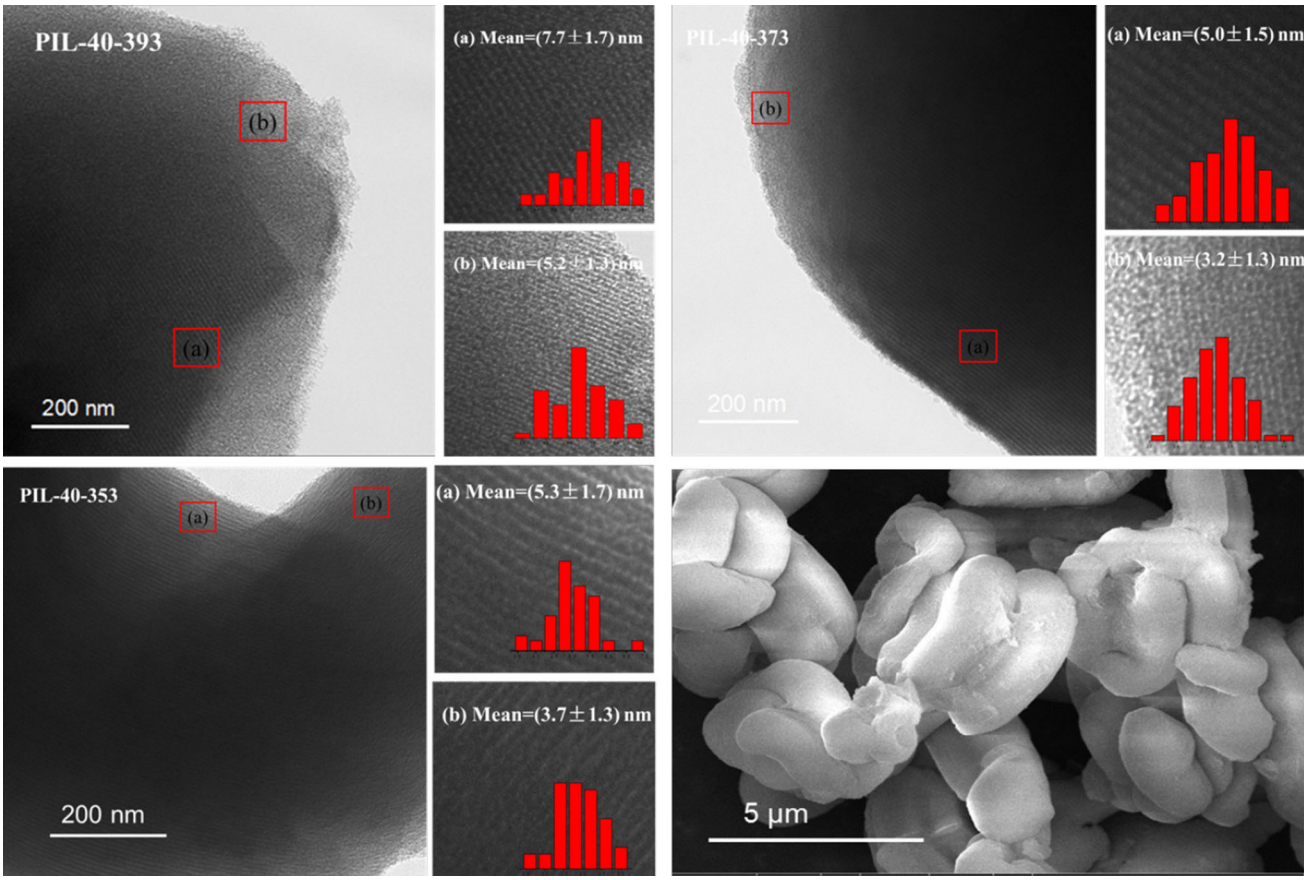

Fig. 6 TEM images of the PIL-40 at different temperature and SEM image of PIL-40-393. The pictures on the right of each image are the local enlargements with the same enlargement scale. *Insets* in each picture are the pore size distribution histograms

Figure 6 shows the TEM images of PIL-40 synthesized at different temperature. Two different kinds of mesoporous channels of all the samples are vividly observed. Moreover, the two different mesoporous channels are arranged in an ordered array. Meanwhile, a little disordered structure obtained at 353 K can be seen which may be caused by the low aging temperature. And all the samples show uniformly distributed pores with the pore size estimated to be 4.0, 7.3 nm from the image, which is in agreement with the result of N_2 gas sorption. A part of the walls of mesoporous channels are destroyed a little in the enlarged picture, which may due to the existence of worm-like micropores. Through the analysis, it is known that the low aging temperature can affect the synthesis of the ordered mesoporous channels. With the increase of the temperature, the materials which not only possess numbers of micropores but also remain the hexagonally ordered array structure are induced. And the materials with two kinds of mesoporous channels with small amounts of micropores can be fabricated at a higher temperature of 393 K. The morphology of the PIL-40 particles prepared at 393 K is shown in the SEM image 6, which exhibits worm-like shapes, and the mesoporous channels can be clearly seen. The worm-like particles have a relatively uniform size (about 4 μm) with a diameter of about 1 μm and tend to aggregate into a wheat-like macroscopic structure.

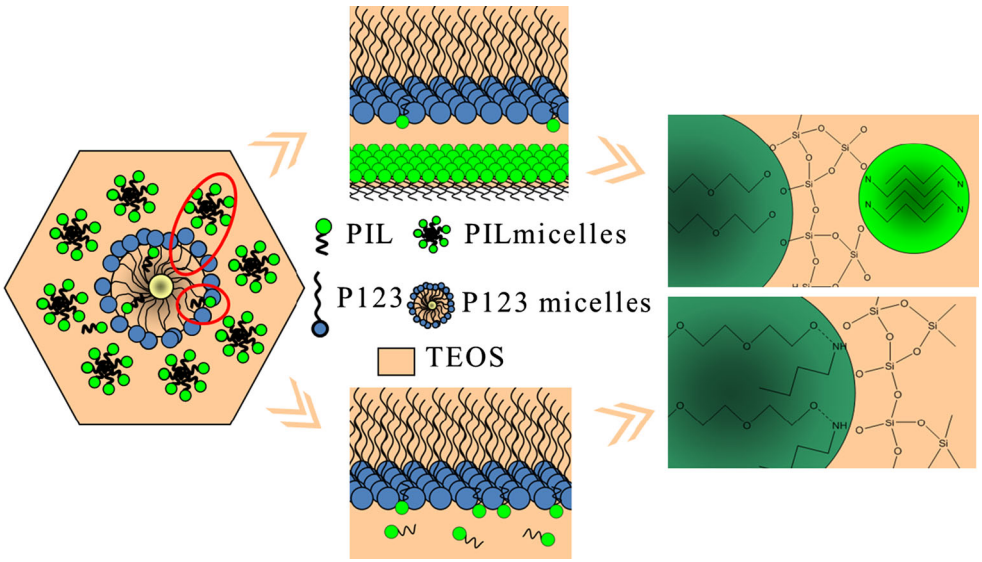

Fig. 7 Postulate mechanism of the micro/mesoporous material with two kinds of mesoporous channels

Formation mechanism of hierarchical micro/mesoporous silica: P123 molecules have the hydrophobic core and the hydrophilic head group and can self-assemble into the mesoscale micelles in aqueous systems. Moreover, ILs can self-assemble into ordered structures like surfactants in an aqueous solution because IL comprises both a hydrophilic ionic headgroup and a hydrophobic organic chain. Furthermore, there is a strong interaction between PIL and P123 mainly due to the hydrogen bond. The micelles with two different sizes are formed because the different size of the PIL molecular and P123 molecular. What is more, the domain size of PIL and the diameter of the P123 cylindrical micelle and PIL micelles control the size of micropores and mesopores. So, the micro/mesoporous material with two different mesoporous diameter is successfully synthesized. The ammonium-based ionic liquid (butylamine acetate) can act as multiple roles of cosolvent, cosurfactant as well as salt in the system. At low PIL concentration, the co-solvent and co-surfactant functions are dominant. PIL and P123 are miscible and can form mixed micelles in aqueous solution. For one thing, the short chains of PIL probably incline to swell the P123 micelles. As a result, the increase of P123/PIL mixed aggregates' diameter is inevitable. For another, PIL can separate from the mixed micelles at higher concentration of protic ionic liquid. And the large micelles with two different sizes lead to the presence of two different kinds of mesopores. This phenomenon is certified by pore size distribution of the samples synthesized at 393 K which have two peaks (4.0, 7.3 nm). The micropores and the mesopores whose pore size is 4.0 nm may generate in the wall of the mesoporous material. And the TEM images and the N_2 adsorption and desorption isothermals give a certainty of the existing of micropores and mesopores in the synthesized porous materials. Meanwhile, it is worth noting that the average diameter of micropore and mesopore will change in a range of 6.5–7.3 nm with the increase of PIL content. And the formation mechanism of the micro/mesoporous silica material which is based on the interaction between PIL and P123 is schematically presented in Fig. 7.

3.3 Catalytic activity of micro/mesoporous materials supported HPW

The IR spectra of the pure HPW, PIL-X and HPW/PIL-X–Y are shown in Fig. 8a. Pure HPW shows IR peaks approximately at 1080 (P-O in the central tetrahedron), 980 (terminal W=O) and 890 and 800 (W–O–W) cm^{-1} corresponding to asymmetric vibration associated with Keggin ion. IR peak of SBA-15 at 3440 cm^{-1} is stretching frequency for hydroxyl and silicon hydroxyl), 1630 cm^{-1} peak is bending vibration peak for O–H of adsorbed water, 461, 808 and 1080 cm^{-1} peaks corresponding to the rocking, bending (or symmetric stretching), and asymmetric stretching of the inter-tetrahedral oxygen atoms in SiO_2 of PIL-X, respectively. Figure 8b presents the IR spectra of all different HPW/PIL-X–Y samples. It can be seen that the IR bands at approximately 980, 890 and 800 cm^{-1} are clearly observed. From the FT-IR analysis, it is found that the primary structure of 12-Tungstophosphoric acid is preserved even after immobilization at the surface of PIL-X–Y.

The catalytic performance of different carriers with HPW were investigated owing to the carriers contain high surface area and narrow size distribution which are favorable conditions for the reaction. It is found that pure HPW shows high catalytic performance for the reaction, however, it is difficult to separate the HPW from the product

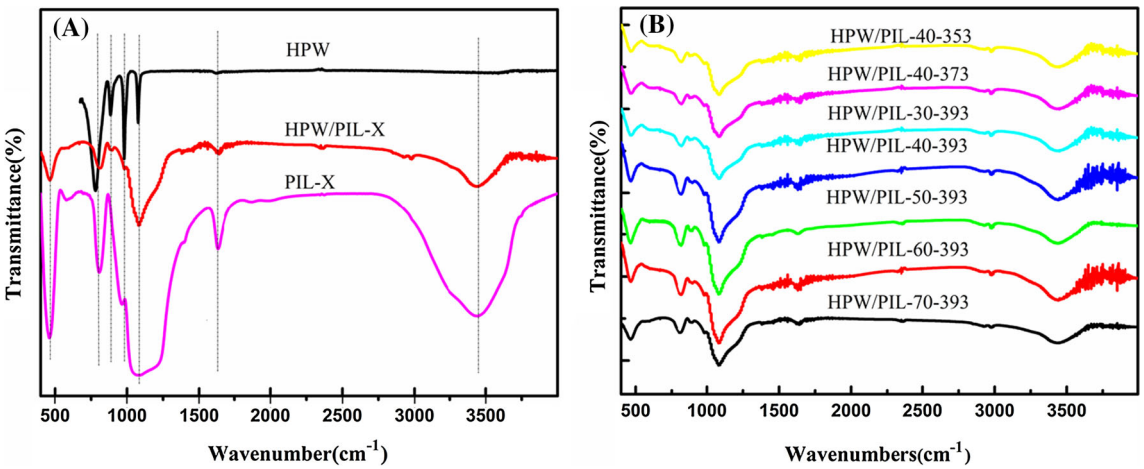

Fig. 8 **a** FT-IR spectra of pure HPW, PIL-X and HPW/PIL-X and **b** FT-IR spectra of different HPW/PIL-X–Y samples

Table 3 Activity of various supported HPW catalysts in alkylation of *o*-xylene with styrene

Catalyst	Yield (%)[a]	Selectivity (%)[b]
HPW	97.9	97.9
PIL-40-393	–	–
HPW/SBA-15	68.2	75.1
HPW/PIL-70-393	83.0	86.3
HPW/PIL-60-393	85.2	89.1
HPW/PIL-50-393	90.9	93.7
HPW/PIL-40-393	90.3	90.6
HPW/PIL-30-393	91.0	94.9
HPW/PIL-40-373	86.6	86.8
HPW/PIL-40-353	80.2	80.4

Reaction conditions: *o*-xylene: styrene = 7.5:1, reaction temperature = 393 K reaction time = 3.0 h, catalyst loading = 20 % (w/w of styrene)

[a] Isolated yield based on the amount of styrene

[b] Target product: all products

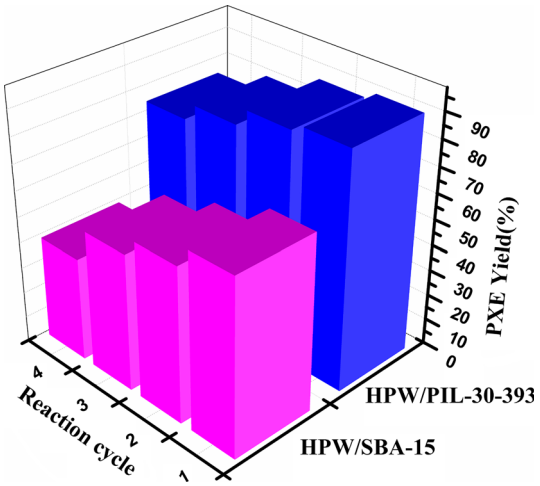

Fig. 9 Catalytic stability of the HPW/PIL-30-393 and HPW/SBA-15 catalysts in the alkylation of *o*-xylene with styrene (Reaction conditions: *o*-xylene: styrene = 7.5:1, reaction temperature = 393 K, reaction time = 3.0 h, catalyst loading = 20 % (w/w of styrene)

mixture. Moreover, the SBA-15 support itself shows no activity performances, which is consistent with literature reports [30]. From Table 3, it can be noted that all the samples exhibit the higher catalytic properties than HPW/SBA-15. Among the catalysts investigated, HPW/PIL-30-393 with large pore size of the support exhibited the best catalytic performance. Therefore, the catalytic activity may change along with the pore size of supports because large pore size material is conducive to the macromolecular reaction. That is to say suitable pore size may contribution to the high catalytic performance.

The important questions that must be addressed while studying alkylation processes over a solid catalyst relate to the stability of the catalyst to leaching of the active component and the possibility of catalyst recycling. The reusability of the HPW/PIL-30-393 and HPW/SBA-15 catalysts has been evaluated by carrying out the reaction with used catalyst under the optimized conditions. After each run, the catalyst was recovered by filtration, then washed with ethanol, dried and calcined at 573 K for 4 h, and used again. From Fig. 9, it can be observed that only 16 % reduction in the activity after 4 runs on the HPW/PIL-30-393 catalyst. In contrast, the deactivation of HPW/SBA-15 catalyst is much faster and PXE yield drops to 40 % after the fourth reaction cycle. HPW/SBA-15 showed a poor catalytic stability may be caused by the possibility that HPW leaching from the catalyst support into the liquid reaction system may result in the low conversion. Furthermore, the special structure of the support with two different kinds of mesoporous channels may be another reason for better stability.

4 Conclusion

In this work, a series of micro/mesoporous silica materials with ordered bimodal mesopores have been successfully fabricated using P123 and PIL (butylamine acetate) as co-templates. And the influence of PIL content and hydrothermal temperature to the structure of the final materials has been investigated systematically. On the basis of the experimental results and the theory analysis, a possible formation mechanism of the micro/mesoporous silica is illustrated. At low PIL concentration, PIL and P123 can form mixed micelles in aqueous solution under the function of the hydrogen bond. PIL may separate from P123 micelles and form mesoscale micelles with the increase of PIL content. The results showed that the sample PIL-40-373 not only possessed a t-plot micropore area of 102 $m^2 g^{-1}$ but also maintained the special ordered structure with two different mesoporous channels of 4.0 and 7.3 nm. Furthermore, the catalytic performances of the micro/mesoporous materials with ordered bimodal mesopores supported HPW catalysts were investigated in the alkylation of *o*-xylene with styrene. Alkylation results showed that catalysts had good activity and reusability, which may be related to the large pore size, the special mesoporous channels of the support and the strong interaction between the HPW and the supports.

Acknowledgments The authors are grateful to the financial supports of National Natural Science Foundation of China (Grant Nos. 21306023, 21376051, 21106017 and 51077013), Fund Project for Transformation of Scientific and Technological Achievements of Jiangsu Province of China (Grant No. BA2011086), Key Program for the Scientific Research Guiding Found of Basic Scientific Research Operation Expenditure of Southeast University (Grant No. 3207043101) and Instrumental Analysis Fund of Southeast University.

References

1. C.T. Kresge, M.E. Leonowicz, W.J. Roth, J.C. Vartuli, J.S. Beck, Nature **359**, 710–712 (1992)
2. Y.S. Ooi, S. Bhatia, Micropor. Mesopor. Mater. **102**, 310–317 (2007)
3. T. Welton, Chem. Rev. **99**, 2071–2083 (1999)
4. J.H. Clark, D.J. Macquarrie, S.J. Tavener, Dalton Trans. 4297–4309 (2006)
5. T.L. Chew, A.L. Ahmad, S. Bhatia, Adv. Compos. Mater **153**, 43–57 (2010)
6. J.L. Vivero-Escoto, I.I. Slowing, B.G. Trewyn, V.S.Y. Lin, Small **6**, 1952–1967 (2010)
7. Y.S. Tao, H. Kanoh, L. Abrams, K. Kaneko, Chem. Rev. **106**, 896–910 (2006)
8. X. Chen, Z.Q. Sun, L.L. Zheng, Z.M. Chen, Y.F. Wang, N. Fu, K. Zhang, X. Yan, H. Liu, L. Jiang, B. Yang, Adv. Mater. **16**, 1632–1636 (2004)
9. K. Egeblad, C.H. Christensen, M. Kustova, C.H. Christensen, Chem. Mater. **20**, 946–960 (2008)
10. A. Noda, A.B. Susan, K. Kudo, S. Mitsushima, K. Hayamizu, M. Watanabe, J. Phys. Chem. B **107**, 4024–4033 (2003)
11. E.E. Yalcinkaya, F.O. Pelit, I. Guney, H. Turkmen, J. Porous Mater. **21**, 1151–1158 (2014)
12. Q.X. Luo, B.W. An, M. Ji, S.E. Park, C. Hao, Y.Q. Li, J. Porous Mater. **22**, 247–259 (2015)
13. Z. Ma, J.H. Yu, S. Dai, Adv. Mater. **22**, 261–285 (2010)
14. P. Hapiot, C. Lagrost, Chem. Rev. **108**, 2238–2264 (2008)
15. K. Binnemans, Chem. Rev. **105**, 4148–4204 (2005)
16. C.K. Lee, H.W. Huang, I.J.B. Lin, Chem. Commun. 1911–1912 (2000)
17. Y. Zhou, M. Antonietti, Adv. Mater. **15**, 1452–1455 (2003)
18. Y. Zhou, J.H. Schattka, M. Antonietti, Nano Lett. **4**, 477–481 (2004)
19. J. Hu, J.X. Yin, T.S. Lin, G.T. Li, J. Chem. Educ. **89**, 284–285 (2012)
20. F. Gao, J. Hu, C.J. Peng, H.L. Liu, Y. Hu, Langmuir **28**, 2950–2959 (2012)
21. A. Kumar, P. Venkatesu, RSC Adv. **3**, 362–367 (2013)
22. T.L. Greaves, A. Weerawardena, C. Fong, I. Krodkiewska, C.J. Drummond, J. Phys. Chem. B **110**, 22479–22487 (2006)
23. S. Tsuzuki, W. Shinoda, M.S. Miran, H. Kinoshita, T. Yasuda, M. Watanabe, J. Chem. Phys. **139**, 174504 (2013)
24. Z.F. Chen, T.L. Greaves, R.A. Caruso, C.J. Drummond, J. Mater. Chem. **22**, 10069–10076 (2012)
25. X.L. Sheng, Y.M. Zhou, Y.W. Zhang, Y.Z. Duan, M.W. Xue, Catal. Lett. **142**, 360–367 (2012)
26. X.L. Sheng, Y.M. Zhou, Y.W. Zhang, M.W. Xue, Y.Z. Duan, Chem. Eng. J. **179**, 295–301 (2012)
27. B.C. Gagea, Y. Lorgouilloux, Y. Altintas, P.A. Jacobs, J.A. Martens, J. Catal. **265**, 99–108 (2009)
28. X.L. Sheng, Y.M. Zhou, Y.L. Yang, Y.W. Zhang, Z.W. Zhang, S.J. Zhou, X.Q. Fu, S. Zhao, RSC Adv. **4**, 30697–30703 (2014)
29. J.Y. Weng, C.M. Wang, H.R. Li, Y. Wang, Green Chem. **8**, 96–99 (2006)
30. X.L. Sheng, J. Kong, Y.M. Zhou, Y.W. Zhang, Z.W. Zhang, S.J. Zhou, Micropor. Mesopor. Mater. **187**, 7–13 (2014)